# Inflammation-dependent cerebrospinal fluid hypersecretion from the choroid plexus epithelium in post-hemorrhagic hydrocephalus

Jason K. Karimy[1*], Jinwei Zhang[1,2*], David B. Kurland[3], Brianna Carusillo Theriault[3], Daniel Duran[1], Jesse A. Stokum,[3] Charuta Gavankar Furey[1], Xu Zhou[4], M. Shahid Mansuri[1], Julio Montejo[1], Alberto Vera[1], Michael L. DiLuna[1], Eric Delpire[5], Seth L. Alper[6], Murat Gunel[1], Volodymyr Gerzanich[3], Ruslan Medzhitov[4], J. Marc Simard[3,7*], and Kristopher T. Kahle[1,8*]

[1]Department of Neurosurgery, Yale School of Medicine, New Haven, CT 06510, USA.
[2]Institute of Biomedical and Clinical Sciences, University of Exeter Medical School, Hatherly Laboratory, Exeter, EX4 4PS, UK.
[3]Department of Neurosurgery, University of Maryland, School of Medicine, Baltimore, MD 21201, USA.
[4]Howard Hughes Medical Institute, Department of Immunobiology, Yale University School of Medicine, New Haven, Connecticut 06520, USA.
[5]Department of Anesthesiology, Vanderbilt University School of Medicine, Nashville, TN, USA.
[6]Division of Nephrology and Vascular Biology Research Center, Beth Israel Deaconess Medical Center; Department of Medicine, Harvard Medical School, Boston, MA, 02215, USA.
[7]Departments of Pathology and Physiology, University of Maryland, School of Medicine, Baltimore, MD 21201, USA.
[8]Departments of Pediatrics and Cellular & Molecular Physiology; and Centers for Mendelian Genomics, Yale School of Medicine, New Haven, CT 06510, USA.

*Equal contributors.

**Corresponding author:**
Kristopher T. Kahle, M.D., Ph.D.
kristopher.kahle@yale.edu

**The choroid plexus epithelium (CPE) secretes higher volumes of fluid (CSF) than any other epithelium and simultaneously functions as the blood-CSF barrier to gate immune cell entry into the CNS.[1] Post-hemorrhagic hydrocephalus (PHH), an expansion of the cerebral ventricles due to CSF accumulation following intraventricular hemorrhage (IVH), is a common disease usually treated by suboptimal CSF shunting techniques.[2] PHH is classically attributed to primary impairments in CSF reabsorption, but little experimental evidence supports this concept. In contrast, the potential contribution of CSF secretion to PHH has received little attention. We demonstrate here that IVH causes a toll-like receptor-4 (TLR4) and NF-κB-dependent inflammatory response of the CPE that is associated with a ~3-fold increase in bumetanide-sensitive CSF secretion. IVH-induced CSF hypersecretion is mediated by the TLR4-dependent activation of the Ste20-type stress kinase SPAK, which binds, phosphorylates, and stimulates the NKCC1 cotransporter at the CPE apical membrane. Genetic depletion of TLR4 or SPAK normalizes hyperactive CSF secretion rates and reduces PHH, as does treatment with drugs that antagonize TLR4-NF-κB signaling or the SPAK-NKCC1 cotransporter complex. These data uncover a previously unrecognized contribution of CSF hypersecretion to the pathogenesis of PHH, demonstrate a novel role for TLRs in regulation of the internal brain milieu, and identify a kinase-regulated mechanism of CSF secretion that could be targeted by repurposed, FDA-approved drugs to treat hydrocephalus.**

IVH frequently leads to PHH, worsening outcomes of germinal matrix and subarachnoid bleeds, and of intraparenchymal hemorrhage.[2] The elevated intracranial pressure (ICP) in PHH damages periventricular white matter, impairing brain development in children and causing neurodegeneration in adults.[3] Severe, persistent elevations in ICP can cause acute brainstem herniation and death. The mainstay of PHH treatment remains invasive CSF shunting, an empiric "one-size-fits-all" approach with high morbidity due to frequent shunt obstructions and infections requiring surgical revision.[2] Targeted pharmacotherapeutic strategies constitute an urgent unmet need for hydrocephalus patients of all ages.[3]

It is widely accepted that PHH results from intraventricular CSF accumulation due to failed homeostasis mechanisms. Classic models of CSF dynamics hold that PHH results from a primary decrease in CSF reabsorption due to intraventricular CSF flow obstruction and/or dysfunction of extraventricular arachnoid granulations; however, this paradigm is supported by sparse experimental evidence,[4] and neglects potential roles of increased CSF secretion in disease pathogenesis.[5] Although intracerebroventricular (ICV) injection of IVH-derived metabolites is sufficient to cause CPE inflammation,[6] and hydrocephalus,[7] the molecular mechanisms by which IVH leads to ventriculomegaly remain incompletely understood.

Systemic secretory epithelia can respond to pro-inflammatory stimuli by *increasing* their rate of fluid secretion.[8] Initially, this secretory response may be adaptive in maintaining homeostasis by clearing pathogenic organisms or debris from the epithelial surface.[9,10] However, sustained inflammation can be maladaptive and create disease vulnerabilities,[11,12] and dysregulated epithelial homeostasis can manifest result in chemical (sterile), autoimmune, and infectious pleuritis, colitis, pancreatitis, and other conditions.[13,14] Interestingly, CSF hypersecretion due to CPE hyperplasia or choroid plexus tumors is sufficient to cause non-obstructive hydrocephalus;[5] however, the impact of IVH on CSF secretion from the CPE has not been studied.

We hypothesized that IVH-induced CPE inflammation might contribute to the development of PHH by increasing the rate of CSF secretion from the CPE. To test this hypothesis, we first assessed CPE inflammation after the experimental simulation of IVH in an established rat model of PHH,[15] induced by intracerebroventricular injection of sterile, LPS-free, autologous blood in 8-week-old, male Wistar rats. Control rats received ICV injection of sterile artificial CSF for comparision.[15] Experimental PHH rats developed ventriculomegaly 48 hours after ICV injection and CPE cells harbored significant activation of NF-κB signaling, as demonstrated by elevated nuclear translocation of p65, a subunit of the NF-κB-p65 transcription complex (Suppl Fig 1). This was accompanied by increased numbers of activated $ED1^+$ (CD68) choroid plexus myeloid cells[15] compared to control rats (Suppl Fig 1 A, B). Intraperitoneal (IP) delivery of the NF-κB inhibitor ammonium pyrrolidinedithiocarbamate (PDTC)[16] lowered IVH-associated increases in p65 nuclear translocation and $ED1^+$ cells (Suppl Fig 1 C). IHC analysis of CPE showed increased expression of NF-κB-p65 and the NF-κB-dependent proteins, TNFα and CD68 (as indicated by ED1), in IVH rats compared to controls at 48h and at 7 days (Suppl Fig 2). Consistent with previous reports,[6,15] these results demonstrate that IVH triggers CPE inflammation dependent on NF-κB activation.

We next evaluated the effect of IVH on the CSF secretion rate from the lateral ventricle CPE using a recently developed direct method of measurement in live rats (Fig 1 A).[17] This method blocks CSF exit from the third ventricle at the level of the Sylvian aqueduct with mineral oil (Fig 1 A). These conditions prevent contributions to measured CSF production via CSF reabsorption pathways distal to this block, including glymphatic pathways or arachnoid granulations near the superior sagittal sinus. Therefore, this technique measures *bona fide* lateral ventricle CSF production (LVCP) by the CPE, as demonstrated previously.[17] 48 hours after ICV injection of blood, LVCP was ~1.40 ± 0.07 μL/min, nearly 3-fold greater than that of either naïve rats or sham-operated controls (~0.50 ± 0.05 μL/min; Fig 1 B; $p < 0.01$). LVCP peaked at 24h post-IVH and remained elevated at 7 days (Fig 1 B). This increase in LVCP was associated with significant ventriculomegaly (Fig 1 C, D; ~2.45 ± 0.05 $mm^3$ in controls versus ~5.40 ± 0.70 $mm^3$ in IVH; $p < 0.01$). Infusion of artificial CSF (aCSF) into the lateral ventricles of naïve rats at a rate of 1 μL/min for 8 hours, approximating the difference in LVCP between IVH and control rats (see Fig 1 C, D), recapitulated the ventriculomegaly seen after IVH (Fig 1 C, D; ~4.90 ± 0.40 $mm^3$; $p < 0.05$ compared to controls; $p > 0.05$ compared to IVH). These data show IVH causes a significant increase in CSF secretion that is sufficient to cause acute PHH.

Ion and water transport molecules expressed on the apical and basolateral membranes of the CPE mediate CSF secretion via the vectorial transport of $Na^+$, $Cl^-$, and $HCO_3^-$ from blood into the ventricles, accompanied by $K^+$ recycling across the apical CPE membrane.[18] We investigated the molecular determinants of IVH-induced CSF hypersecretion. ICV delivery of acetazolamide to inhibit carbonic anhydrase (CA) isoforms that regenerate $HCO_3^-$ only mildly lowered IVH-induced CSF hypersecretion (Fig 1 E). Systemic administration of PDTC to inhibit NF-κB decreased CSF hypersecretion and ventriculomegaly after IVH (Fig 1 E; CSF: ~45% reduction, $p < 0.01$; Fig 2 G; ventriculomegaly: ~55% decrease, $p < 0.01$). ICV (but not systemic) delivery of bumetanide, an inhibitor of cation-$Cl^-$-cotransporter NKCC1, significantly reduced post-IVH CSF hypersecretion and ventriculomegaly (Fig 1 F-G; CSF: ~80% reduction at 48h and ~70% reduction at 7 days; $p < 0.01$; Fig 1 G; ventriculomegaly: ~50% reduction, $p < 0.01$). These

results demonstrate that CSF hypersecretion after IVH is sensitive to inhibitors of inflammation (PDTC) and NKCC1-dependent ion transport.

We evaluated the expression of specific CPE ion transporter polypeptides in the presence or absence of IVH using Western blotting of CPE homogenates fractionated by SDS-PAGE. IVH significantly increased the functional expression of NKCC1, detected as "pNKCC1" (the active, ion-transporting species phosphorylated at residues P-Thr$^{203}$/P-Thr$^{207}$/P-Thr$^{212}$)[19] (Fig 2 A, B; ~6.8-fold activation, $p < 0.01$). In contrast, protein expression of AQP1 and the $Na^+/K^+$ ATPase (including $Na^+/K^+$ ATPase P-Ser$^{23}$) were mildly decreased ($p < 0.05$) in the setting of IVH (Fig 2 A, B).

In other cell types, the conserved C-terminal domain (CCT) of the serine-threonine STE20/SPS1-related, proline alanine-rich kinase (SPAK) associates with the (R/K)FX(V/I) motif of NKCC1 and phosphorylates its N-terminus at Thr$^{203}$, Thr$^{207}$, and Thr$^{212}$.[20] Like other Ste20-type kinases that serve as MAP4Ks, SPAK integrates and transduces environmental stress,[20] including NF-κB-dependent inflammatory signals.[21,22] Given the IVH-induced increase in both NKCC1 P-Thr$^{203}$/P-Thr$^{207}$/P-Thr$^{212}$ and bumetanide-sensitive CSF secretion, we tested the effect of IVH on SPAK expression using total and phospho-specific antibodies on CPE homogenates (Fig 2 A, B). Similar to NKCC1, IVH significantly increased the functional expression of SPAK (SPAK P-Ser$^{373}$ "pSPAK") > 2-fold ($p < 0.01$) relative to that in control animals (Fig 2 A, B).

Reciprocal co-immunoprecipitation experiments from CPE homogenates using total and phospho-specific anti-SPAK antibodies and anti-NKCC1 antibodies each showed that SPAK and NKCC1 form a physical complex in the CPE (Fig 2 C). This complex includes the phosphorylated and active species of each (pSPAK and pNKCC1) (Fig 2 C, D). The interaction between pSPAK and pNKCC1 was increased in the setting of IVH (Fig 2 C, D). Consistent with our Western and co-immunoprecipitation results, immunohistochemistry on CPE sections labeled with anti-pSPAK and anti-pNKCC1 antibodies showed a significant increase in pSPAK and pNKCC1 at the apical membrane of the CPE after IVH (Fig 2 E, F). Treatment with the NF-κB inhibitor PDTC blocked the IVH-dependent up-regulation of pSPAK-pNKCC1 after IVH (Fig 2 E, F).

We applied pharmacological and genetic approaches to test the *functional* contribution of pSPAK-pNKCC1 to development of PHH. ICV administration of STOCK1S-50699, which disrupts binding between SPAK and NKCC1,[23] restored CSF secretion rates after IVH to basal levels (Fig 2 G; CSF: ~50%; $p < 0.01$). Closantel, which directly inhibits SPAK kinase activity,[24] restored CSF secretion rates to basal levels and normalized ventricular size after IVH (Fig 2 G; CSF: ~65%; $p < 0.01$; Fig 2 H, I; ventriculomegaly: ~40%, $p < 0.05$). STOCK1S-50699 and closantel were administered either ICV at the time of CSF measurement or ICV via osmatic pump at the time of IVH for ventriculomegaly analysis (see Methods). ICV delivery of SPAK antisense oligodeoxyribonucleotides (AS-ODNs), but not scrambled control ODNs (Scr-ODNs; see Methods), decreased levels of both SPAK and pNKCC1 (Suppl Fig 3), and attenuated IVH-induced CSF hypersecretion (Fig 2 G; ~45%; $p < 0.01$). These data show that chemical or genetic inhibition of SPAK-NKCC1 complex decreases IVH-induced CSF hypersecretion and ventriculomegaly.

We next explored the upstream mechanisms that mediate CPE inflammation and pSPAK-pNKCC1 up-regulation after IVH. Toll-like receptor-4 (TLR4)-/NF-κB signaling is a critical mediator of the innate immune response to bacteria-derived lipopolysaccharide (LPS),[25] but is also activated by other *host*-derived "alarmins" or damage-associated molecular patterns (DAMPs), including sterile blood metabolites.[26] TLR4 is expressed in CPE cells,[27] but the role for TLR in the pathogenesis of PHH is unclear. We tested the effect of TLR4 inhibition on IVH-induced up-regulation of pSPAK-pNKCC1 using the specific TLR4 inhibitor, Tak242[28] (Fig 3 A, E) and TLR4 KO rats (Fig 3 B, F).

IVH activated TLR4 signaling, as evidenced by up-regulation of TAK1 p-Thr187 (~2-fold, $p < 0.05$), NF-κB-p65 (up to 9-fold, $p < 0.05$), and pNF-κB-p65 (p-Ser536) (> 90-fold, $p < 0.05$) at 24h and 48h post-IVH, and to a lesser extent at 7 days post-IVH (Fig 3 A, B). These changes were accompanied by increased pSPAK (~2-fold, $p < 0.01$) and pNKCC1 (~6-fold, $p < 0.01$) (Fig 3A, C). Tak242 abrogated the IVH-induced activation of TLR4 signaling and the activating phosphorylation of both pSPAK ($p < 0.01$) and pNKCC1 ($p < 0.01$) (Fig 3 A, E). TLR4 KO also abolished the IVH-induced activation of TLR4 signaling and the up-regulation of pSPAK ($p < 0.01$) and pNKCC1 ($p < 0.01$) (Fig 3 B, F). In contrast, expression of the $Na^+/K^+$ ATPase and AQP1 was mildly decreased at 24h post-IVH, and restored 7 days post-IVH ($p < 0.05$).

We next assessed the role of TLR4 inhibition on IVH-induced CSF hypersecretion using Tak242 or TLR4 KO rats (Fig 3 G). In contrast to the increased rates of CSF secretion measured in TLR4 WT rats in response to IVH, CSF secretion rates in TLR4 KO rats were not significantly different from those in control animals (Fig 3 G; CSF: ~70% reduction, $p < 0.01$). Consistent with this, Tak242 also decreased CSF hypersecretion at 48h post-IVH (Fig 3 G; CSF: ~53% reduction, $p < 0.01$). These data demonstrate TLR4 is required for IVH-induced CSF hypersecretion associated with CPE inflammation.

The data presented here offer several novel insights (Suppl Fig. 4). *First*, IVH triggers CSF hypersecretion by the CPE, uncovering a previously unrecognized contribution of increased CSF secretion to the pathogenesis of PHH. *Second*, IVH-induced CPE inflammation and CSF hypersecretion is dependent on TLR4-NFκB signaling, demonstrating a novel role for TLRs in the regulation of the internal brain milieu. *Third*, TLR4-NFκB stimulates CSF hypersecretion via the SPAK-NKCC1 cotransporter complex, identifying a novel kinase-regulated mechanism of CSF secretion.

SPAK kinase is a master regulator of epithelial ion transporters and channels,[20] including the cation-$Cl^-$ cotransporters[29]. In the nervous system, SPAK is most highly expressed in the CPE, where it localizes to the apical CPE membrane.[30] We showed that SPAK and NKCC1 form a complex in the CPE, and that the phosphorylated, active species of each is increased after IVH. SPAK loss-of-function in the distal nephron results in low blood pressure from epithelial NaCl wasting[31] due to *decreased* phosphorylation of the furosemide-sensitive NKCC2, a renal-specific NKCC1 homologue. We have shown the opposite phenomenon in PHH. After IVH, SPAK gain-of-function in the CPE results in PHH from CSF hypersecretion due to *increased* phosphorylation of the bumetanide-sensitive NKCC1 at Thr residues homologous to those in NKCC2. These findings are consistent with the homology of ion transporters and their regulatory networks in the CPE and nephron.[18] Elucidation of other ion and water transporters and their

regulators that coordinate with NKCC1 to mediate the CSF hypersecretory response could identify other therapeutic targets.

SPAK-NKCC1-mediated CSF hypersecretion is dependent on TLR4/NF-κB signaling. SPAK is a signal transducer of environmental and cellular stress,[20] including NF-κB-dependent inflammation.[21,22] IFN-γ[32] and TNF-α[22] stimulate SPAK signaling in an NF-κB-dependent manner to increase epithelial transport in experimental colitis.[32] SPAK could therefore be well positioned to mediate a TLR4/NF-κB-dependent epithelial *"pro-secretory response"* to inflammation. While CSF hypersecretion from the CPE after IVH may resemble the hypersecretory phenotype in other inflamed epithelia,[13,14] it is poorly tolerated given the ventricular system's confinement within the rigid skull, where even small elevations in CSF volume can create fatal increases in intracranial pressure.

TLR4 inhibition decreases inflammatory injury and neurological deficits after intraparenchymal hemorrhage,[33] and TLR4 and its downstream pathway components (NF-κB, and the NF-κB-dependent cytokines TNFα and IL-1β) are up-regulated in the CPE after IVH.[6] It has been reported that IVH-derived metabolites, such as heme[33] and methemoglobin,[34] serve as DAMPs to bind and activate TLR4. Our results corroborate these findings, and further suggest that specific IVH-derived metabolites may serve as CSF-borne host-derived DAMPs that induce TLR4/NF-κB signaling in the CPE. These findings suggest post-infectious hydrocephalus (PIH), a devastating complication of meningitis from LPS-producing bacteria, could result from similar TLR4-dependent CSF hypersecretory mechanisms. Such a mechanistic similarity could be of great importance, since PIH is the most common type of hydrocephalus worldwide (including the developing world, where neurosurgeons are scarce and the costs of VP shunting are prohibitive).[35] Future study into the normal and pathophysiological roles of TLRs in the CPE will be important topics of investigation.

Previous trials failed to show efficacy of systemically administered furosemide or acetazolamide for the treatment of PHH associated with neonatal germinal matrix hemorrhage.[36] However, furosemide and bumetanide have poor blood-brain barrier (BBB) penetration, and furosemide has significantly lower affinity for NKCC1 than bumetanide.[37] ICV[38] but not intraperitoneal,[39] delivery of the NKCC1 blocker bumetanide moderately decreases *baseline* CSF secretion in dogs, but bumetanide has not been studied in the context of PHH. We showed IVH-induced CSF hypersecretion and hydrocephalus is sensitive to ICV but not systemic bumetanide. This is consistent with the low BBB permeability of bumetanide[37] and the post-IVH increase in pNKCC1 at the apical CPE membrane.

Importantly, patients with PHH often require acute placement of *temporary* external ventricular drains or reservoirs to divert CSF and decrease elevated intracranial pressures before placement of a permanent in-dwelling VP-shunt several weeks later. Although endoscopic cauterization of the CPE has proven effective in some forms of infantile hydrocephalus,[40] that efficacy may come at the expense of other critical and increasingly recognized functions of the CPE such as immune surveillance, growth factor production, and vitamin homeostasis.[1] In contrast, acute ICV delivery of repurposed drugs targeting either TLR4-NF-κB-dependent inflammation or the SPAK-NKCC1 complex might serve as a novel strategy to avoid permanent shunt dependence while preserving other critical "non-secretory" CPE functions.

ACKNOWLEDGENTS

We thank D. R. Alessi (Dundee) and R.P. Lifton (Rockefeller) for their support. K.T.K. is supported by the March of Dimes Basil O'Connor Award, a Simons Foundation SFARI Grant, the Hydrocephalus Association Innovator Award, and the NIH (4K12NS080223-05). J.M.S. is supported by the National Institute of Neurological Disorders and Stroke (NINDS) (NS060801; NS061808) and the U.S. Department of Veterans Affairs (1BX002889); R.M. is supported by the Howard Hughes Medical Institute. The authors have no competing interests.

AUTHOR CONTRIBUTIONS:

K.T.K., J.M.S., V.G., and J.K.K. conceived and designed the study. J.K.K, J.Z., D.B.K., B.C.T., and J.A.S. preformed molecular and physiological experiments, and data analysis for IVH surgery, genetic and pharmacological drug treatment, CSF secretion measurement, western blot, IHC, and ventricular volume analysis. K.T.K., J.M.S., J.Z., D.D., C.G.F, and J.K.K. drafted the manuscript and figures. X.Z., M.S.M., J.M., A.V., M.L.D., E.D., S.L.A., M.G., and R.M. provided expertise and collaboration in drafting the manuscript. All authors contributed to critical editing and data presentation within the manuscript. J.M.S. and K.T.K are the principal investigators and responsible for the oversight of this study.

FIGURE LEGENDS

FIGURE 1. Intraventricular hemorrhage (IVH) triggers inflammation-dependent and bumetanide-sensitive cerebrospinal fluid (CSF) hypersecretion by the choroid plexus epithelium (CPE).

(A) Left panel shows a schematic of the method of *in vivo* quantification of CSF secretion in a live rat model of post-hemorrhagic hydrocephalus. Yellow depicts a catheter injecting mineral oil into the fourth ventricle and cerebral aqueduct, causing an obstruction to CSF flow. [17] Blue represents a capillary tube inserted into the lateral ventricle proximal to this site of oil block that collects CSF secreted from the lateral ventricle CPE. Right upper panel shows stereotactic injection of into the lateral ventricle through a small parietal craniotomy. Right lower panel shows the direct measurement of CSF secretion in a live Wistar rat. Left arrow highlights the catheter used for mineral oil delivery; right arrow highlights the capillary tube and ruler used for quantitation of CSF secretion.
(B) CSF secretion rates in control rats (CTL, n = 12) and in rats 24hr (n = 3), 48hr (n = 13), 72hr (n = 3) and 7 days (d) (n = 3) after IVH. Bars represent mean ± SEM of the rate of CSF secretion (μL/min). Symbols indicate data obtained from an individual animal. *, $p < 0.05$ vs. control rats (CTL), one-way ANOVA.
(C) Representative photomicrographs of coronal sections of rat brains (at -0.6 mm from Bregma) that depict ventricular volume under various experimental conditions. N = naïve; CTL = vehicle injection; IVH = 48 hr post-experimental IVH; aCSF = 8 hr after a 1 μL/min infusion of artificial CSF to approximate the difference in CSF secretion at 48 hr post-IVH. Note the similarity of ventricular size after aCSF injection or IVH. Scale bar = 3.5 mm.
(D) Graph depicting the mean ± SEM of lateral ventricle volume ($mm^3$) in naïve rats (N, n=3), in control rats (CTL) which received vehicle injection only (n = 3), in rats 48 hours after IVH (IVH, n = 3), and in rats 8 hours after a 1μL/min infusion of artificial CSF (aCSF) (n = 5). *, $p < 0.01$ vs control; #, $p < 0.05$ vs control but not vs. IVH ($p > 0.05$); one-way ANOVA.
(E) Effect of intracerebroventricular (ICV) administration of the carbonic anhydrase inhibitor acetazolamide (ACZ), the NKCC1 cotransporter inhibitor bumetanide (BUM), and intraperitoneal (IP) administration of the NF-kB inhibitor Ammonium pyrrolidinedithiocarbamate (PDTC) on the rate of CSF secretion 48 hours post-experimental IVH. The graph represents the mean ± SEM (n=3) of the rate of CSF secretion (μL/min). *, $p < 0.01$ vs. control (CTL); #, $p < 0.01$ vs. IVH but not vs. controls ($p > 0.05$); one-way ANOVA). Veh = ICV injection of vehicle.
(F) Effect of intravenous (IV) injection of BUM 48 hours after experimental IVH. Note the absence of significant CSF secretion change after systemic administration of BUM, but not after ICV administration.
(G) Effect of ICV administration of BUM in rats 48 hours and 7 days after experimental IVH. The graphs represent the mean ± SEM (n=3) of rates of CSF secretion (μL/min). *, $p< 0.05$ vs. minus BUM; paired t-test.

FIGURE 2. CSF hypersecretion after IVH is dependent on the inflammation-induced phospho-activation of the SPAK-NKCC1 complex in the CPE.

(A) Western Blot analysis of CPE ion transporters in control rats and rats 48 hours after experimental IVH. CPE lysates (n=3) were harvested and subjected to SDS-PAGE and to immunoblot with the indicated antibodies. Molecular mass is indicated in kDa. The blots in the figure have been cropped for presentation, please see supplemental information to view the uncropped blots. CTL = control rats; IVH = 48 hours post-experimental IVH. pSPAK = phosphorylated (active) SPAK; pOSR1= phosphorylated (active) OSR1 kinase; pNKCC1 = phosphorylated (active) NKCC1. AQP1 = aquaporin-1.
(B) Graphs representing the β-Actin-normalized Western blot signal from panel (A) (mean ± SEM), as quantified in Methods. *, $p < 0.05$ vs. control; one-way ANOVA. CTL = control rats; IVH= 48 hours post-experimental IVH.
(C) Reciprocal co-immunoprecipitation of CPE lysates with anti-pSPAK and anti-pNKCC1 antibodies. Upper panel: immunoblot against total NKCC1 and SPAK. Bottom panel: immunoblot against pNKCC1 and pSPAK. The blots in the figure have been cropped for presentation, please see supplemental information to view the uncropped blots. Molecular mass is indicated in kDa.
(D) Reciprocal co-immunoprecipitation experiments with anti-SPAK and anti-NKCC1 specific antibodies in the CPE. Lysates from CPE were prepared (n=3) and subjected to immunoprecipitation (IP) and immunoblot (IB) after SDS-PAGE with the indicated antibodies. The blots in the figure have been cropped for presentation, please see supplemental information to view the uncropped blots. Molecular mass is indicated in kDa.
(E) Representative fluorescent photomicrographs immunolabeled for pSPAK (green) and pNKCC1 (red) using phospho-specific antibodies that detect the activated, phosphorylated species of each molecule in the CPE of rats 48 hours after treatment with vehicle control (CTL) or experimental IVH in the presence or absence of the NF-κB inhibitor PDTC. DAPI staining shown in blue. Scale bar = 200 μm.
(F) Graphs depicting the mean ± SEM of the fluorescence quantification (ROI%) (see Methods) from fluorescent photomicrographs immunolabeled for pSPAK (upper panel) and pNKCC1 (lower panel) as in (E) *, $p < 0.01$ vs. control; #, $p < 0.05$ vs. IVH but not vs. control ($p > 0.05$); one-way ANOVA.
(G) Effect of genetic or pharmacologic inhibition of SPAK on IVH-induced CSF hypersecretion from the CPE. The graph represents mean ± SEM of the rate of CSF secretion (μL/min). *, $p < 0.01$ vs. control; #, $p < 0.01$ vs. IVH but not vs. controls ($p > 0.05$); one-way ANOVA. ODN= oligodeoxyribonucleotide; Scr=Scrambled; AS=Anti-sense; Veh = Vehicle injection; STK = STOCK 1S-50699; Clos = Closantel.
(H) Representative photomicrographs of coronal sections of brains (at -0.6 mm from Bregma) (left panel) from vehicle control rats (CTL) or in rats 48 hours after experimental IVH in the presence of ICV-delivered drugs. Scale bar = 3.5 mm.
(I) Graph depicting the mean ± SEM of lateral ventricular volume ($mm^3$) from rats as indicated in (H). *, $p < 0.01$ vs. control; #, $p < 0.01$ vs. IVH but not vs. control ($p > 0.05$); one-way ANOVA.

FIGURE 3. TLR4-NF-κB signaling is required for the IVH-induced increase in SPAK-NKCC1-dependent CSF hypersecretion.
(A) Western Blot analysis of CPE ion mediators in control rats and rats 24 hr, 48 hr, and 7d after experimental IVH in the presence or absence of Tak242 (n=3). CPE lysates were harvested and

subjected to immunoblot with the indicated antibodies. The blots in the figure have been cropped for presentation, please see supplemental information to view the uncropped blots. Molecular mass is indicated in kDa. CTL = control rats; IVH = post-experimental IVH. pSPAK = phosphorylated (active) SPAK; pOSR1= phosphorylated (active) OSR1 kinase; pNKCC1 = phosphorylated (active) NKCC1; TAK1 = Transforming growth factor beta-activated kinase; pTAK1= phosphorylated TAK1; $pNa^+/K^+$ ATPase = phosphorylated $Na^+/K^+$ ATPase; AQP1 = aquaporin-1.

(B) Western Blot analysis of CPE ion transport mediators in TLR4 wild-type (TLR4 WT) animals and TLR4 knockout (TLR4 KO) animals 48 hours after experimental IVH (n=3). The blots in the figure have been cropped for presentation, please see supplemental information to view the uncropped blots.

(C, D) Graphs representing the mean ± SEM of the β-Actin-normalized Western blot signal of the indicated antigen as depicted in triplicate columns 1, 2, 4 and 5 of panel (A). *, $p < 0.05$ vs. control; one-way ANOVA (n=3).

(E) Graph representing the mean ± SEM of the ratio of the β-Actin-normalized Western blot signal of the indicated antigen as depicted in the third triplicate column of panel (A), demonstrating the effect of TAK242 treatment on CPE ion transport mediators 48 hours post experimental IVH. *, $p < 0.05$ vs. control; #, $p < 0.01$ vs. IVH but not vs. controls ($p > 0.05$); one-way ANOVA (n=3).

(F) Graph representing the mean ± SEM of the β-Actin-normalized Western blot signal of the indicated antigen as depicted in (B), demonstrating lack of ion transporter up-regulation in TLR4 KO animals. Graph contains a break from 2 to 7 on the Y-axis to accommodate elevated expression of pNKCC1 in the IVH condition.

(G) Graph depicting CSF secretion rates (μL/min) 48 hours after experimental IVH, in TLR4 WT untreated animals, in TLR4 WT animals treated with TAK242, and in TLR4 KO animals.

## References


1. Lun, M.P., Monuki, E.S. & Lehtinen, M.K. Development and functions of the choroid plexus-cerebrospinal fluid system. *Nat Rev Neurosci* **16**, 445-457 (2015).
2. Kahle, K.T., Kulkarni, A.V., Limbrick, D.D., Jr. & Warf, B.C. Hydrocephalus in children. *Lancet* **387**, 788-799 (2016).
3. McAllister, J.P., 2nd*, et al.* An update on research priorities in hydrocephalus: overview of the third National Institutes of Health-sponsored symposium "Opportunities for Hydrocephalus Research: Pathways to Better Outcomes". *Journal of neurosurgery* **123**, 1427-1438 (2015).
4. Chen, Q.*, et al.* Post-hemorrhagic hydrocephalus: Recent advances and new therapeutic insights. *Journal of the neurological sciences* **375**, 220-230 (2017).
5. Karimy, J.K.*, et al.* Cerebrospinal fluid hypersecretion in pediatric hydrocephalus. *Neurosurg Focus* **41**, E10 (2016).
6. Gram, M.*, et al.* Extracellular hemoglobin - mediator of inflammation and cell death in the choroid plexus following preterm intraventricular hemorrhage. *Journal of neuroinflammation* **11**, 200 (2014).
7. Gao, C.*, et al.* Role of red blood cell lysis and iron in hydrocephalus after intraventricular hemorrhage. *Journal of cerebral blood flow and metabolism : official journal of the International Society of Cerebral Blood Flow and Metabolism* **34**, 1070-1075 (2014).
8. Berkes, J., Viswanathan, V.K., Savkovic, S.D. & Hecht, G. Intestinal epithelial responses to enteric pathogens: effects on the tight junction barrier, ion transport, and inflammation. *Gut* **52**, 439-451 (2003).
9. Wilson, R.*, et al.* Upper respiratory tract viral infection and mucociliary clearance. *European journal of respiratory diseases* **70**, 272-279 (1987).
10. Doyle, W.J.*, et al.* Nasal and otologic effects of experimental influenza A virus infection. *The Annals of otology, rhinology, and laryngology* **103**, 59-69 (1994).
11. Kotas, M.E. & Medzhitov, R. Homeostasis, inflammation, and disease susceptibility. *Cell* **160**, 816-827 (2015).
12. Nowarski, R., Jackson, R. & Flavell, R.A. The Stromal Intervention: Regulation of Immunity and Inflammation at the Epithelial-Mesenchymal Barrier. *Cell* **168**, 362-375 (2017).
13. Sin, B. & Togias, A. Pathophysiology of allergic and nonallergic rhinitis. *Proceedings of the American Thoracic Society* **8**, 106-114 (2011).
14. Thiagarajah, J.R., Donowitz, M. & Verkman, A.S. Secretory diarrhoea: mechanisms and emerging therapies. *Nat. Rev. Gastroenterol. Hepatol* **12**, 446-457 (2015).
15. Simard, P.F.*, et al.* Inflammation of the choroid plexus and ependymal layer of the ventricle following intraventricular hemorrhage. *Translational stroke research* **2**, 227-231 (2011).
16. Liu, S.F., Ye, X. & Malik, A.B. Inhibition of NF-kappaB activation by pyrrolidine dithiocarbamate prevents In vivo expression of proinflammatory genes. *Circulation* **100**, 1330-1337 (1999).
17. Karimy, J.K.*, et al.* A novel method to study cerebrospinal fluid dynamics in rats. *J. Neurosci. Methods* **241**, 78-84 (2015).
18. Damkier, H.H., Brown, P.D. & Praetorius, J. Cerebrospinal fluid secretion by the choroid plexus. *Physiol Rev* **93**, 1847-1892 (2013).
19. Vitari, A.C.*, et al.* Functional interactions of the SPAK/OSR1 kinases with their upstream activator WNK1 and downstream substrate NKCC1. *The Biochemical journal* **397**, 223-231 (2006).
20. Gagnon, K.B. & Delpire, E. Molecular physiology of SPAK and OSR1: two Ste20-related protein kinases regulating ion transport. *Physiol Rev* **92**, 1577-1617 (2012).

21. Piechotta, K., Garbarini, N., England, R. & Delpire, E. Characterization of the interaction of the stress kinase SPAK with the Na+-K+-2Cl- cotransporter in the nervous system: evidence for a scaffolding role of the kinase. *The Journal of biological chemistry* **278**, 52848-52856 (2003).
22. Yan, Y., *et al.* Nuclear factor-kappaB is a critical mediator of Ste20-like proline-/alanine-rich kinase regulation in intestinal inflammation. *The American journal of pathology* **173**, 1013-1028 (2008).
23. de Los Heros, P., *et al.* The WNK-regulated SPAK/OSR1 kinases directly phosphorylate and inhibit the K+-Cl- co-transporters. *The Biochemical journal* **458**, 559-573 (2014).
24. Kikuchi, E., *et al.* Discovery of Novel SPAK Inhibitors That Block WNK Kinase Signaling to Cation Chloride Transporters. *J. Am. Soc. Nephrol* **26**, 1525-1536 (2015).
25. Medzhitov, R. TLR-mediated innate immune recognition. *Seminars in immunology* **19**, 1-2 (2007).
26. Miyake, K. Innate immune sensing of pathogens and danger signals by cell surface Toll-like receptors. *Seminars in immunology* **19**, 3-10 (2007).
27. Skipor, J., Szczepkowska, A., Kowalewska, M., Herman, A.P. & Lisiewski, P. Profile of toll-like receptor mRNA expression in the choroid plexus in adult ewes. *Acta veterinaria Hungarica* **63**, 69-78 (2015).
28. Kawamoto, T., Ii, M., Kitazaki, T., Iizawa, Y. & Kimura, H. TAK-242 selectively suppresses Toll-like receptor 4-signaling mediated by the intracellular domain. *European journal of pharmacology* **584**, 40-48 (2008).
29. Alessi, D.R., *et al.* The WNK-SPAK/OSR1 pathway: master regulator of cation-chloride cotransporters. *Science signaling* **7**, re3 (2014).
30. Piechotta, K., Lu, J. & Delpire, E. Cation chloride cotransporters interact with the stress-related kinases Ste20-related proline-alanine-rich kinase (SPAK) and oxidative stress response 1 (OSR1). *J. Biol. Chem* **277**, 50812-50819 (2002).
31. Yang, S.S., *et al.* SPAK-knockout mice manifest Gitelman syndrome and impaired vasoconstriction. *J Am Soc Nephrol* **21**, 1868-1877 (2010).
32. Yan, Y., Nguyen, H., Dalmasso, G., Sitaraman, S.V. & Merlin, D. Cloning and characterization of a new intestinal inflammation-associated colonic epithelial Ste20-related protein kinase isoform. *Biochimica et biophysica acta* **1769**, 106-116 (2007).
33. Lin, S., *et al.* Heme activates TLR4-mediated inflammatory injury via MyD88/TRIF signaling pathway in intracerebral hemorrhage. *Journal of neuroinflammation* **9**, 46 (2012).
34. Kwon, M.S., *et al.* Methemoglobin is an endogenous toll-like receptor 4 ligand-relevance to subarachnoid hemorrhage. *International journal of molecular sciences* **16**, 5028-5046 (2015).
35. Boivin, M.J., Kakooza, A.M., Warf, B.C., Davidson, L.L. & Grigorenko, E.L. Reducing neurodevelopmental disorders and disability through research and interventions. *Nature* **527**, S155-160 (2015).
36. Whitelaw, A., Kennedy, C.R. & Brion, L.P. Diuretic therapy for newborn infants with posthemorrhagic ventricular dilatation. *The Cochrane database of systematic reviews*, Cd002270 (2001).
37. Romermann, K., *et al.* Multiple blood-brain barrier transport mechanisms limit bumetanide accumulation, and therapeutic potential, in the mammalian brain. *Neuropharmacology* **117**, 182-194 (2017).
38. Javaheri, S. & Wagner, K.R. Bumetanide decreases canine cerebrospinal fluid production. In vivo evidence for NaCl cotransport in the central nervous system. *The Journal of clinical investigation* **92**, 2257-2261 (1993).
39. Vogh, B.P. & Langham, M.R., Jr. The effect of furosemide and bumetanide on cerebrospinal fluid formation. *Brain research* **221**, 171-183 (1981).
40. Stone, S.S. & Warf, B.C. Combined endoscopic third ventriculostomy and choroid plexus cauterization as primary treatment for infant hydrocephalus: a prospective North American series. *Journal of neurosurgery. Pediatrics* **14**, 439-446 (2014).

Competing financial interest statements (CFI)

After careful review, the authors in the manuscript have no competing financial interests that could potentially undermine our objectivity, integrity, or the perceived value of this publication. This includes, but is not limited to, funding sources, employment, stocks in companies, or consulting.

Signed: Jason K. Karimy, M.S. 05/18/2017

## ONLINE METHODS

### Animals

Animal experiments were performed under a protocol approved by the Institutional Animal Care and Use Committee (IACUC) of the University of Maryland, and in accordance with the guidelines and regulations in the NIH Guide for the Care and Use of Laboratory Animals. Male Wistar rats (Harlan, Indianapolis, IN, USA), or *Tlr4*$^{-/-}$ rats[41] (bred in accordance with IACUC protocol at the University of Maryland, Baltimore), age 8 weeks (220-230g), were anesthetized (60 mg/kg ketamine plus 7.5 mg/kg xylazine, IP) and allowed to breathe room air spontaneously. Body temperature was maintained at 37 ± 1°C (Harvard Apparatus, Holliston, MA, USA) throughout the course of the experiments. Animals in this study were randomly chosen for either control or experimental conditions, the researchers were not blinded, and no animals were excluded.

### Model of post-hemorrhagic hydrocephalus

IVH was modeled using a modified protocol based on previously described methods.[42,43] In an anesthetized animal, the tail artery was aseptically cannulated using a flexible catheter (PE-20) pre-loaded with heparinized saline. The rat was then mounted in a stereotactic apparatus (Stoelting Co., Wood Dale, IL), a midline scalp incision was made to expose the skull and a 1 mm burr hole was made using a high-speed drill over the right lateral ventricle (coordinates, x= -0.8, y= -1.7 mm relative to bregma). Approximately 200 µL of blood was then drawn from the tail artery catheter and loaded into a 500 µL syringe (Hamilton, Reno, NV), which was then mounted to the stereotactic frame. Under stereotactic guidance, 50 µL of freshly collected autologous blood, free from anticoagulants, was infused into the right lateral ventricle (coordinates, x= -0.8, y= -1.7, z= -4.5 mm relative to bregma), over the course of 5 minutes, and the 26-gauge needle was held in place for an additional 20 minutes to prevent backflow of blood upon needle removal. Intraventricular infusion of sterile aCSF (Tocris, Bristol, UK) in the same manner served as the control condition.

### Quantitation of rates of CSF production

Rates of CSF production were measured using the method we recently published.[44] Briefly, anesthetized rats were mounted in a stereotactic apparatus and a 1.3 mm burr hole was made over the left lateral ventricle (coordinates, x= -0.8, y= +1.7 relative to bregma). Next, the rat's head was rotated on the ear-bars 90$^{o}$, nose-down, and the suboccipital muscles were dissected to the cisterna magna to expose the atlanto-occipital ligament. The ligament was punctured and a 23-gauge flexible catheter (PE-20) was advanced 5 mm through the foramen of Magendie to the 4th ventricle. Sterile, molecular grade mineral oil (100 µL; Sigma Aldrich, St. Louis, MO) was infused into the 4th ventricle to occlude the aqueduct of Slyvius, thereby creating a closed system of CSF circulation. With the rat in the same position, a glass capillary tube (cat # CV8010-300; borosilicate; OD, 1 mm; ID, 0.8 mm; length, 30 cm; VitroCom, Mountain Lakes, NJ) was advanced through the burr hole into the left lateral ventricle. The volume (V) of CSF that formed at a given timepoint was calculated as: $V\ (mm^3) = \pi \cdot r^2 \cdot d$, where r is the radius of the capillary tube and d is the distance CSF traveled within the capillary. The rate of CSF formation (µL/min) could be calculated from the slope of the volume–time relationship.

### Ventricular volume analysis

Following IP injection of pentobarbital, rats were transcardially perfused with ice-cold normal saline followed by 10% neutral buffered formalin. The brains were harvested, kept in formalin for 24 hours at 4°C and then cryoprotected (30% sucrose). To prevent distortion from cryosectioning and slide mounting, we took high resolution pictures of serial coronal sections (200 μm apart, 14 levels) while the brain was mounted in the cryostat, using uniform parameters of camera positioning, magnification, and external lighting. Adobe Photoshop was used to obtain a pixel count of the lateral ventricular area in each thick section. Pixels were converted to area in $mm^2$, summed over 14 levels and multiplied by the distance between levels (0.2 mm) to calculate ventricular volume.

8hr aCSF infusion

In anesthetized naïve rats, a 28-gauge cannula from an Alzet brain infusion kit (#1; Durect, Cupertino, CA), with a single spacer to adjust the depth to 4.5 mm, was stereotactically placed in the burr hole over the right lateral ventricle and secured to the skull using cyanoacrylate adhesive. A solution of aCSF was infused at 1 μL/min over the course of 8 hours. At the end of 8 hours, the rat was euthanized and transcardially perfused and processed for ventricular volume analysis as described above.

Immunohistochemistry

Rats were transcardially perfused with ice-cold normal saline followed by 10% neutral buffered fomalin. Brains were harvested and kept in formalin for 24 hours before being transferred to a 30% sucrose solution for cryoprotection. Brains were cryosectioned (10μm, coronal), blocked (2% donkey serum, +0.2% Triton X-100 for 1 hour at RT) then incubated overnight at 4°C with primary antibodies. Sections were washed three times in phosphate-buffered saline and incubated for 1 hour at RT with secondary antibodies (1:500; Alexa Fluor 488 and Alexa Fluor 555; Invitrogen, Molecular Probes, Eugene, OR, USA). Sections were coverslipped using a polar mounting medium containing 4'6-diamidino-2-phenylindole (DAPI; Invitrogen, Eugene, OR, USA) and analyzed with epifluorescence microscopy (Nikon Eclipse 90i; Nikon Instruments Inc., Melville, NY, USA). Quantitation was performed by regions of interest (ROI) using NIS-Elements AR software (Nikon Instruments Inc., Melville, NY, USA) and specific signal was defined as > 2 x background.

Choroid plexus protein isolation and immunoprecipitation

*Buffers.* Buffer A contained 50 mM Tris/HCl, pH7.5 and 0.1 mM EGTA. Lysis buffer was 50 mM Tris/HCl, pH 7.5, 1 mM EGTA, 1 mM EDTA, 50 mM sodium fluoride, 5 mM sodium pyrophosphate, 1 mM sodium orthovanadate, 1% (w/v) NP-40, 0.27 M sucrose, 0.1% (v/v) 2-mercaptoethanol and protease inhibitors (1 tablet per 50 ml). TBS-Tween buffer (TTBS) was Tris/HCl, pH 7.5, 0.15 M NaCl and 0.2% (v/v) Tween-20. SDS sample buffer was 1X-NuPAGE LDS sample buffer (Invitrogen), containing 1% (v/v) 2-mercaptoethanol.

*Isolation.* Choroid plexuses were harvested rapidly from adult rat brains following transcardial perfusion with ice-cold saline. The brain was isolated and then placed in an ice-cold saline bath, after which the choroid plexus was carefully dissected under magnification using sharp forceps. Approximately 3 mg of choroid plexus tissue was harvested from one brain, which was then collected into a 1.5 mL tube.

Immunoblotting and immunoprecipitation.

Clarified lysates of CP membrane fraction (15 µg) in SDS sample buffer were subjected to electrophoresis on polyacrylamide gels and transferred to nitrocellulose membranes. The membranes were incubated for 30 min with TTBS containing 5% (w/v) skim milk. The membranes were then immunoblotted in 5% (w/v) skim milk in TTBS with the indicated primary antibodies overnight at 4°C. Sheep antibodies were used at a concentration of 1-2 µg/ml. The incubation with phospho-specific sheep antibodies was performed in the presence of 10 µg/ml of the dephospho-peptide antigen to ensure phospho-antigen specificit. The blots were then washed six times with TTBS and incubated for 1 hour at room temperature with secondary HRP-conjugated antibodies diluted 5000-fold in 5% (w/v) skim milk in TTBS. After repeating the washing steps, the signal was detected with enhanced chemiluminescence reagent. Immunoblots were developed using a film automatic processor (SRX-101; Konica Minolta Medical) and films were scanned with a 600-dpi resolution on a scanner (PowerLook 1000; UMAX). Figures were generated using Photoshop/Illustrator (Adobe). The relative intensities of immunoblot bands were determined by densitometry with ImageJ software. NKCC1 and SPAK were immunoprecipitated from the indicated cell extracts. 0.2 mg of the indicated clarified cell extract was incubated with 15 µg of the indicated antibody conjugated to 15 µl of protein-G–Sepharose. Incubation was for 2 hours at 4°C with gentle agitation, and the immunoprecipitates were washed three times with 1 ml of lysis buffer containing 0.15 M NaCl and twice with 1 ml of buffer A. Bound proteins were eluted with 1x lithium dodecyl sulfate (LDS) sample buffer (see "Antibodies for Western blot and immunoprecipitation" below for greater detail).

ICV drug treatment

The technique described previously for the administration of ICV drugs while measuring the rate of CSF secretion was used.[44] Briefly, at the time of CSF collection, before rotating the head to a vertical orientation, a 28-gauge cannula from an Alzet brain infusion kit (#1; Durect, Cupertino, CA), with a single spacer to adjust the depth to 4.5 mm, was stereotactically placed in the burr hole over the right lateral ventricle and secured to the skull using cyanoacrylate adhesive. The cannula was connected via a preloaded PE-20 catheter to a 1 mL syringe containing the drug solution (see below). The syringe was loaded into a syringe infusion apparatus (Pump elite 11, Harvard Apparatus) and maintained at 37°C. To determine rate of CSF formation during intraventricular drug infusion, the "actual infusion rate" of the drug (1.93 µL/min) was subtracted from the "measured outflow rate" to obtain the operational "calculated rate of CSF formation". To assess the effect of a drug, the baseline rate of CSF formation was determined during spontaneous CSF formation (no drug infusion), then the calculated rate of formation was determined after switching to the test drug. Percent change (Δ%) was determined using the formula: $\Delta\% = \frac{(calculated\ rate)-(baseline\ rate)}{baseline\ rate}$. Intraventricular infusion solutions were made using artificial CSF (aCSF), composed as follows (in mM): Na 150; K 3.0; Ca 1.4; Mg 0.8; P 1.0; Cl 155, pH 7.19 (Tocris, Bristol, UK), with a calculated osmolarity of 311.2 mOsmC/L. The following drugs were used: acetazolamide (45 mM, pH 9; Sigma Aldrich, St. Louis, MO), STOCK-1S 50699 (100 µM, pH 6, 1% DMSO), Closantel (30 µM, pH 7.2, 0.1% DMSO; Sigma Aldrich) and Bumetanide (2.7 mM, pH 9; Sigma Aldrich). Due to differences in drug solubility, each drug had a specific vehicle control to account for pH, DMSO co-solvent, and osmolarity to ensure that these differences did not alter rate of CSF production. For each control solution, aCSF solution was altered using NaOH and HCl (Sigma Aldrich), to adjust pH, and mannitol (Sigma Aldrich), to adjust the osmolarity. In each case, the vehicle controls had no statistical

effect on the baseline rate of CSF and therefore, a representative vehicle control will be presented in data analysis for simplicity of data presentation.

Systemic ammonium pyrrolidinedithiocarbamate (PDTC) administration

PDTC (100mg/kg in normal saline, IP, Sigma Aldrich) was administered IP at the time of IVH surgery and every 8 hours thereafter until 48 hours post IVH. At 48 hours following IVH, rats were either (i) euthanized and transcardially perfused with saline and 10% neutral buffered formalin and processed for immunohistochemistry analysis, as described above, or (ii) anesthetized for surgery to allow measurement of the rate of CSF secretion, described above.

Systemic bumetanide administration

The efficacy of systemic bumetanide administration was determined by IV infusion of bumetanide at the time of measuring the rate of CSF production. In an anesthetized rat, the internal jugular vein was exposed and catheterized using a PE-20 flexible catheter preloaded with sterile normal saline. The rat was then mounted into a stereotactic frame in the normal manner for the CSF measurement analysis described above. A baseline measurement of the rate of CSF production was calculated for 25 minutes. After the baseline rate was determined, the saline-filled syringe attached to the jugular catheter was removed and replaced with a bumetanide-loaded syringe (1 mg/mL in pH 9 normal saline), and 1 mL was infused over 1 minute. Following bumetanide infusion, CSF measurement was continued for an addition 30 minutes to detect any changes in the rate of production.

Systemic TAK-242 administration

TAK-242 (ethyl (6R)-6-[N-(2-chloro-4-fluorophenyl)sulfamoyl]cyclohex-1-ene-1-carboxylate) was purchased from Sigma Aldrich. The concentration of TAK-242 chosen for intravenous administration (1mg/kg/hr; pH 7.2; 10% (2-Hydroxypropyl)-β-cyclo-dextrin in normal saline; 0.5% DMSO) was based on previous studies demonstrating the half-life[45] and efficacy of drug[46-48] at a concentration range of 0.5 – 1 mg/kg in rats. TAK-242 was dissolved in 100% DMSO for stock solutions and diluted with 10% (2-Hydroxypropyl)-β-cyclo-dextrin in normal saline (pre-warmed to 37˚C) for working solutions to a final concentration of 0.5% DMSO. TAK-242 solution was loaded into an Alzet osmotic pump (2ML1; Durect, Cupertino, CA). In an anesthetized rat, the internal jugular vein was exposed and catheterized using a PE-20 flexible catheter preloaded with the TAK-242 solution connected to the alzet pump. The catheter was secured into place, and the pump was implanted subcutaneously on the back. 5 days following TAK-242 pump implantation, the rats were anesthetized and subjected to the model of IVH as described above. The TAK-242 treatment continued over the next 48 hours at which point, the rat either underwent CSF secretion measurements or choroid plexus harvest for western blot analysis.

*In vivo* knockdown of SPAK

Previously validated SPAK antisense oligodeoxynucleotides (ODN; Integrated DNA Technologies, Coralville, IA) were used for in vivo knockdown of SPAK.[49] ODNs were reconstituted in sterile normal saline and diluted to a final concentration of 0.5 μg/μL for ICV injection. All solutions were sterile-filtered. The rats were injected ICV under stereotactic guidance with a 10 μL bolus of either SPAK or scrambled ODN every 12h starting 24h prior to IVH and continued until 48hr following IVH. The sequences were as follows: SPAK,

GG*CTCC*GCC*ATG*ATGC*TGC; scrambled, CGC*TCG*ATCC*AGG*TCA*GCG (* denotes position of locked nucleic acids). To validate the ability of ODNs to knockdown SPAK, IHC was used to detect SPAK and pNKCC1 in naïve rats and in 24 hr IVH rats treated with either scrambled or anti-SPAK ODN.

Antibodies for IHC

The following primary antibodies were used: rabbit anti-SPAK (1:200; Cell Signaling Technology, Danvers, MA; Catalog #2281); rabbit anti-phosphorylated SPAK (pSPAK, Ser 373, 1:200, EMD Millipore, Billerica, MA; Catalog #07-2273); rabbit anti-NKCC1 (1:200, Abcam, Cambridge, MA, Catalog #ab59791); rabbit anti-phosphorylated NKCC1 (pNKCC1, Thr 212/Thr 217, 1:200, EMD Millipore; Catalog #ABS1004); rabbit anti-NFκB/p65 (1:200, Santa Cruz, Dallas, TX; Catalog #sc-372); mouse anti-ED1 (1:100, EMD Millipore; Catalog #MAB1435); goat anti-TNFα (1:200, Santa Cruz; Catalog #sc-1350); goat anti-IBA1 (1:200, Abcam, Catalog #ab5076). Protein was detected using species-appropriate, fluorophor-labeled secondary antibodies (Cell Signaling Technology).

Antibodies for Western blot and immunoprecipitation

The following antibodies were raised in sheep and affinity-purified on the appropriate antigen by the Division of Signal Transduction Therapy Unit at the University of Dundee: NKCC1 total antibody [residues 1-288 of human NKCC1, Catalog S022D]; NKCC1 phospho-$Thr^{203}/Thr^{207}/Thr^{212}$ antibody [residues 198-217 of human NKCC1 phosphorylated at $Thr^{203}$, $Thr^{207}$ and $Thr^{212}$, HYYYD(T)HTN(T)YYLR(T)FGHNT, Catalog S763B]; SPAK-mouse antibody [2–76 of mouse SPAK, Catalog S668D]; SPAK/OSR1 (S-motif) phospho-$Ser^{373}/Ser^{325}$ antibody [367–379 of human SPAK, RRVPGS(S)GHLHKT, which is highly similar to residues 319–331 of human OSR1 in which the sequence is RRVPGS(S)GRLHKT, Catalog S670B). β-Actin (8H10D10) Mouse antibody, Phospho-NF-κB p65 (Ser536) antibody (Catalog #3031), NF-κB p65 (D14E12) antibody (Catalog #8242), $Na^+,K^+$-ATPase antibody (Catalog #3010) and phospho-$Na^+,K^+$-ATPase α1 (Ser23) antibody (Catalog #4006) were purchased from Cell Signaling Technology. TLR4 antibody (L-14) (Catalog sc-16240) and AQP1 antibody (Catalog sc-9878) were purchased from Santa Cruz Biotechnology, Inc.. NFκB p105 / p50 antibody (Catalog ab31412), TAK1 (phospho T187) antibody (Catalog ab192443) and TAK1 antibody (Catalog ab25879) were purchased from Abcam. Horseradish peroxidase-coupled secondary antibodies for immunoblotting were obtained from Pierce. SPAK and NKCC1 total antibodies and the phosphorylation site-specific antibodies were coupled with protein-G–Sepharose at a ratio of 1 mg of antibody per 1 mL of beads in the presence of 20 μg/mL of lysate to which the corresponding non-phosphorylated peptide had been added. 200 μg of clarified cell lysate were incubated with 10 μg of antibody conjugated to 10 μL of protein-G–Sepharose for 2 hours at 4°C with gentle agitation. Beads were washed three times with 1 mL of lysis buffer containing 0.15 M NaCl and twice with 1 mL of wash buffer (50 mM Tris/HCl, pH7.5 and 0.1mM EGTA). Bound proteins were eluted with 1X LDS sample buffer (Invitrogen) containing 1% (v/v) 2-mercaptoethanol. IgG used in control immunoprecipitation experiments was affinity-purified from pre-immune serum using Protein G-Sepharose.

Data Analysis

All statistics were completed in OriginPro (OriginLab Corporation, Northampton, MA) using one-way ANOVA analysis with a Tukey post-hoc test for differences between groups, two-

sample t-test, or paired t-test. Statistical information including exact sample size, f-values, t-valves, and degrees of freedom for all analyses are presented below organized by the corresponding figure. P-values less than 0.0001 are represented in scientific notation, e.g. 1E-04. Numerical data in text and figures are given as mean ± standard error of the mean (SE). Rates (μL/min) were calculated as the slope of the volume-time relationship, based on data collected over 30 min or more. Rates were determined for individual animals and were averaged across individuals. Sample size calculations were based on two previous studies that used the same model of IVH[42] and the method for measuring rates of CSF production.[44] Sample sizes were calculated using an *a priori* sample size calculator with the following assumptions: α=0.05; two-tailed; desired power, 80%; anticipated effect size (Cohen's d), 3. Calculations indicate that a minimum of 3 rats per group would be required. Statistical methods were reviewed and approved by the consultants at StatsLab at Yale University School of Medicine.

Figure 1B: Sample sizes: CTL n=12; 24hr IVH n=3; 48hr IVH n=13; 72hr IVH n=3; 7d IVH n=3.
One-way ANOVA: F-value = 30.53; degrees of freedom (df) = 33. P-values: 24hr IVH vs. CTL = 1.50E-07; 48hr IVH vs. CTL = 2.51E-08; 72hr IVH vs. CTL = 2.22E-04; 7d IVH vs. CTL = 0.015. Figure 1D: Sample sizes: Naive (N), Vehicle control (CTL), IVH: n=3; aCSF n=5. One-way ANOVA: F-value = 14.43; df = 13. P-values: CTL vs. Naïve = 0.86; IVH vs. CTL = 0.007; aCSF vs. CTL = 0.01; aCSF vs. IVH = 0.85. Figure 1E: Sample sizes: CTL n=12; IVH n=13; IVH + PDTC n=3. One-way ANOVA: F-valve = 48.78; df = 27. P-values: IVH vs. CTL = 0; IVH + PDTC vs. CTL = 0.16; IVH + PDTC vs. IVH = 8.35E-04. Sample sizes: IVH + Vehicle n=3; IVH + ACZ n=3; IVH + BUM n=3. One-way ANOVA: F-value = 40.66; df = 8. P-values: ACZ vs. Veh = 0.21; BUM vs. Veh = 3.35E-04; BUM vs. ACZ = 0.001. Figure 1F: Sample size: n=3. Paired T-test; Two-tailed: T-value = -1.11; df = 2. P-value: 0.38 Figure 1G: Sample size: 48hr IVH n=5. Paired T-test; two-tailed: T-value = 12.79; df = 4. P-value: 2.15E-04. Sample size: 7d IVH n=3. Paired T-test; two-tailed: T-value = 12.79; df = 3. P-value: 0.02

Figure 2B: Sample size n=3 all conditions. Two sample T-test; two-tailed; df = 4: all conditions.
pSPAK: T-value = -7.49, P-value = 0.0017; SPAK: T-value = -0.36; P-value = 0.74. pNKCC1: T-value = -16.01, P-value = 8.90E-05; NKCC1: T-value = -0.59; P-value = 0.59. pOSR1: T-value = -5.98, P-value = 0.004; $pNa^+/K^-$ ATPase: T-value = 17.67, P-value = 6.02E-05. $Na^+/K^-$ ATPase: T-value = 11.83, P-value = 2.92E-04; AQP1: T-value = 5.35, P-value = 0.006. Figure 2F: Sample sizes: CTL n=4; IVH n=4; IVH + PDTC n=3. One-way ANOVA: pSPAK: F-value = 14.80; df = 10. pNKCC1: F-value = 15.07; df = 10. P-values: pSPAK: IVH vs. CTL = 0.012; IVH + PDTC vs. CTL = 0.26; IVH + PDTC vs. IVH = 0.002. pNKCC1: IVH vs. CTL = 0.002; IVH + PDTC vs. CTL = 0.13; IVH + PDTC vs. IVH = 0.049. Figure 2G: Sample sizes: CTL = 12; IVH + Scr = 5; IVH + AS = 5. One-way ANOVA: F-value = 19.98; df = 21. P-values: IVH + Scr vs. CTL = 1.39E-05; IVH + AS vs. CTL = 0.44; IVH + AS vs. IVH + Scr = 0.0012. Sample sizes: Veh, STK, Clos n=3 all conditions. One-way ANOVA: F-value = 38.66; df = 8. P-values:

IVH + Veh vs. IVH + STK = 0.0015; IVH + Clos vs. IVH + Veh = 3.83E-04; IVH + Clos vs. IVH + STK = 0.21. Figure 2I: Sample sizes: CTL n=3; IVH n=3; IVH + BUM n=4; IVH + PDTC n=3; IVH + Clos n=3. One-way ANOVA: F-value = 12.21; df = 15. P-values: IVH vs. CTL = 0.0011; IVH + BUM vs. CTL = 1; IVH + BUM vs. IVH = 6.70E-04; IVH + PDTC vs. CTL = 1; IVH + PDTC vs. IVH = 0.0011; IVH + Clos vs. CTL = 0.74; IVH + Clos vs. IVH = 0.007.

Figure 3C: Sample sizes: n=3 all conditions. One-way ANOVA: pSPAK: F-value = 53.04; df = 11; P-values: 24hr IVH vs. CTL = 1.52E-05; 48hr IVH vs. CTL = 3.99E-05; 7d IVH vs. CTL = 0.004. pNKCC1: F-value = 23.85; df = 11; P-values: 24hr IVH vs. CTL = 2.91E-04; 48hr IVH vs. CTL = 6.11E-04; 7d IVH vs. CTL = 0.022. NFκB: F-value = 21.36; df = 11; P-values: 24hr IVH vs. CTL = 4.10E-04; 48hr IVH vs. CTL = 0.003; 7d IVH vs. CTL = 0.27. AQP1: F-value = 16.9; df = 11; P-values: 24hr IVH vs. CTL = .033; 48hr IVH vs. CTL = .1; 7d IVH vs. CTL = 0.056. Figure 3D: Sample sizes: n=3 all conditions. One-way ANOVA: pTAK: F-value = 9.60; df = 11; P-values: 24hr IVH vs. CTL = .0067; 48hr IVH vs. CTL = .045; 7d IVH vs. CTL = 0.88. TAK: F-value = 1.92; df = 11; P-values: 24hr IVH vs. CTL = 0.99; 48hr IVH vs. CTL = 0.20; 7d IVH vs. CTL = 0.63. p$Na^+/K^-$ ATPase: F-value = 5.80; df = 11; P-values: 24hr IVH vs. CTL = 0.019; 48hr IVH vs. CTL = 0.080; 7d IVH vs. CTL = 0.49. $Na^+/K^-$ ATPase: F-value = 5.52; df = 11; P-values: 24hr IVH vs. CTL = 0.23; 48hr IVH vs. CTL = 0.11; 7d IVH vs. CTL = 0.69. Figure 3E: Sample sizes: n=3 all conditions. One-way ANOVA: pSPAK: F-value = 207.98; df = 11; P-values: IVH vs. CTL = 4.03E-06; TAK242 + IVH vs. CTL = 0.30; TAK242 + IVH vs. IVH = 7.12E-06. pNKCC1: F-value = 89.48; df = 11; P-values: IVH vs. CTL = 6.72E-05; TAK242 + IVH vs. CTL = 0.94; TAK242 + IVH vs. IVH = 5.65E-05. pTAK: F-value =14.58; df = 11; P-values: IVH vs. CTL = 0.017; TAK242 + IVH vs. CTL = 0.51; TAK242 + IVH vs. IVH = 5.07E-03. NFκB: F-value = 20.05; df = 11; P-values: IVH vs. CTL = 0.0023; TAK242 + IVH vs. CTL = 0.044; TAK242 + IVH vs. IVH = 0.0079. AQP1: F-value = 3.51; df = 11; P-values: IVH vs. CTL = 0.27; TAK242 + IVH vs. CTL = 0.089; TAK242 + IVH vs. IVH = 0.67. Figure 3F: Sample sizes: n=3 all conditions. One-way ANOVA: pSPAK: F-value = 40.09; df = 11; P-values: IVH vs. CTL = 6.69E-04; TLRKO + IVH vs. CTL = 0.94; TLRKO + IVH vs. IVH = 5.29E-04. pNKCC1: F-value = 52.05; df = 11; P-values: IVH vs. CTL = 3.14E-04; TLRKO + IVH vs. CTL = 0.96; TLRKO + IVH vs. IVH = 2.63E-04; pTAK: F-value = 95.75; df = 11; P-values: IVH vs. CTL = 5.34E-05; TLRKO + IVH vs. CTL = 0.97; TLRKO + IVH vs. IVH = 4.79E-05. NFκB: F-value = 10.34; df = 11; P-values: IVH vs. CTL = .022; TLRKO + IVH vs. CTL = 0.94; TLRKO + IVH vs. IVH = 0.015; AQP1: F-value = 31.92; df = 11; P-values: IVH vs. CTL = 0.0017; TLRKO + IVH vs. CTL = 7.99E-04; TLRKO + IVH vs. IVH = 6.41E-01. Figure 3G: Sample sizes: CTL n=12; IVH n=3; TAK242 + IVH n=3; TLRKO + IVH n=3. One-way ANOVA: F-value = 15.30; df = 20. P-values: IVH vs. CTL = 3.31E-05; TAK242 + IVH vs. CTL 0.67; TAK242 + IVH vs. IVH = 0.003; TLRKO + IVH vs. CTL 0.87; TLRKO + IVH vs. IVH = 1.42E-04.

Supplemental Figure 1D: p65: Sample sizes: CTL n=3; IVH n=4; IVH + PDTC n=5. One-way ANOVA: F-value = 89.78; df = 11. P-values: IVH vs. CTL = 4.27E-06; IVH + PDTC vs. CTL = 0.90; IVH + PDTC vs. IVH = 1.95E-06. ED1: Sample sizes: n=3 all conditions. One-way ANOVA: F-value = 92.37; df = 8. P-values: IVH vs. CTL = 3.93E-05; IVH + PDTC vs. CTL = 0.29; IVH + PDTC vs. IVH = 8.96E-05.

Supplemental Figure 2B: Sample sizes: CTL n=5; 48hr IVH n=5; 7d IVH n=6; all conditions. One-way ANOVA: pSPAK: F-value = 42.46; df = 15; P-values: 48hr IVH vs. CTL = 0.001; 7d IVH vs. CTL = 1.20E-06. pNKCC1: F-value = 8.25; df = 15; P-values: 48hr IVH vs. CTL = 0.047; 7d IVH vs. CTL = 0.004. p65: F-value = 46.81; df = 15; P-values: 48hr IVH vs. CTL = 6.35E-05; 7d IVH vs. CTL = 7.93E-07. TNFα: F-value = 8.05; df = 15; P-values: 48hr IVH vs. CTL = 0.016; 7d IVH vs. CTL = 0.007. IBA1: F-value = 4.71; df = 15; P-values: 48hr IVH vs. CTL = 0.032; 7d IVH vs. CTL = 0.072. ED1: F-value = 6.42; df = 15; P-values: 48hr IVH vs. CTL = 0.067; 7d IVH vs. CTL = 0.01.

## References


41. Ferguson, C., McKay, M., Harris, R.A. & Homanics, G.E. Toll-like receptor 4 (Tlr4) knockout rats produced by transcriptional activator-like effector nuclease (TALEN)-mediated gene inactivation. Alcohol (Fayetteville, N.Y.) 47, 595-599 (2013).
42. Simard, P.F., et al. Inflammation of the choroid plexus and ependymal layer of the ventricle following intraventricular hemorrhage. Translational stroke research 2, 227-231 (2011).
43. Lodhia, K.R., Shakui, P. & Keep, R.F. Hydrocephalus in a rat model of intraventricular hemorrhage. Acta neurochirurgica. Supplement 96, 207-211 (2006).
44. Karimy, J.K., et al. A novel method to study cerebrospinal fluid dynamics in rats. J. Neurosci. Methods 241, 78-84 (2015).
45. Jinno, F., et al. Investigation of the unique metabolic fate of ethyl (6R)-6- [N- (2-chloro-4-fluorophenyl) sulfamoyl] cyclohex-1-ene-1-carboxylate (TAK-242) in rats and dogs using two types of 14C-labeled compounds having different labeled positions. Arzneimittel-Forschung 61, 458-471 (2011).
46. Garate, I., et al. Toll-like 4 receptor inhibitor TAK-242 decreases neuroinflammation in rat brain frontal cortex after stress. Journal of neuroinflammation 11, 8 (2014).
47. Feng, Y., et al. Neuroprotective Effects of Resatorvid Against Traumatic Brain Injury in Rat: Involvement of Neuronal Autophagy and TLR4 Signaling Pathway. Cellular and molecular neurobiology 37, 155-168 (2017).

48. Su, F., et al. Protective effect of ginsenosides Rg1 and Re on lipopolysaccharide-induced sepsis by competitive binding to Toll-like receptor 4. Antimicrobial agents and chemotherapy 59, 5654-5663 (2015).
49. Nugent, B.M., Valenzuela, C.V., Simons, T.J. & McCarthy, M.M. Kinases SPAK and OSR1 are upregulated by estradiol and activate NKCC1 in the developing hypothalamus. The Journal of neuroscience : the official journal of the Society for Neuroscience 32, 593-598 (2012).

Data Availability:

All materials and associated protocols can be found within the methods section of this paper, or the papers referenced.

For addition explanations of the IVH protocol please see published works on Pubmed:
Simard, P.F., et al. Inflammation of the choroid plexus and ependymal layer of the ventricle following intraventricular hemorrhage. Translational stroke research 2, 227-231 (2011).
Lodhia, K.R., Shakui, P. & Keep, R.F. Hydrocephalus in a rat model of intraventricular hemorrhage. Acta neurochirurgica. Supplement 96, 207-211 (2006).

For a detailed protocol on the direct methods of CSF measurement, please see publication on Pubmed:
Karimy, J.K., et al. A novel method to study cerebrospinal fluid dynamics in rats. J. Neurosci. Methods 241, 78-84 (2015).

Any additional information can be addressed via contact with the corresponding article of this manuscript.

884

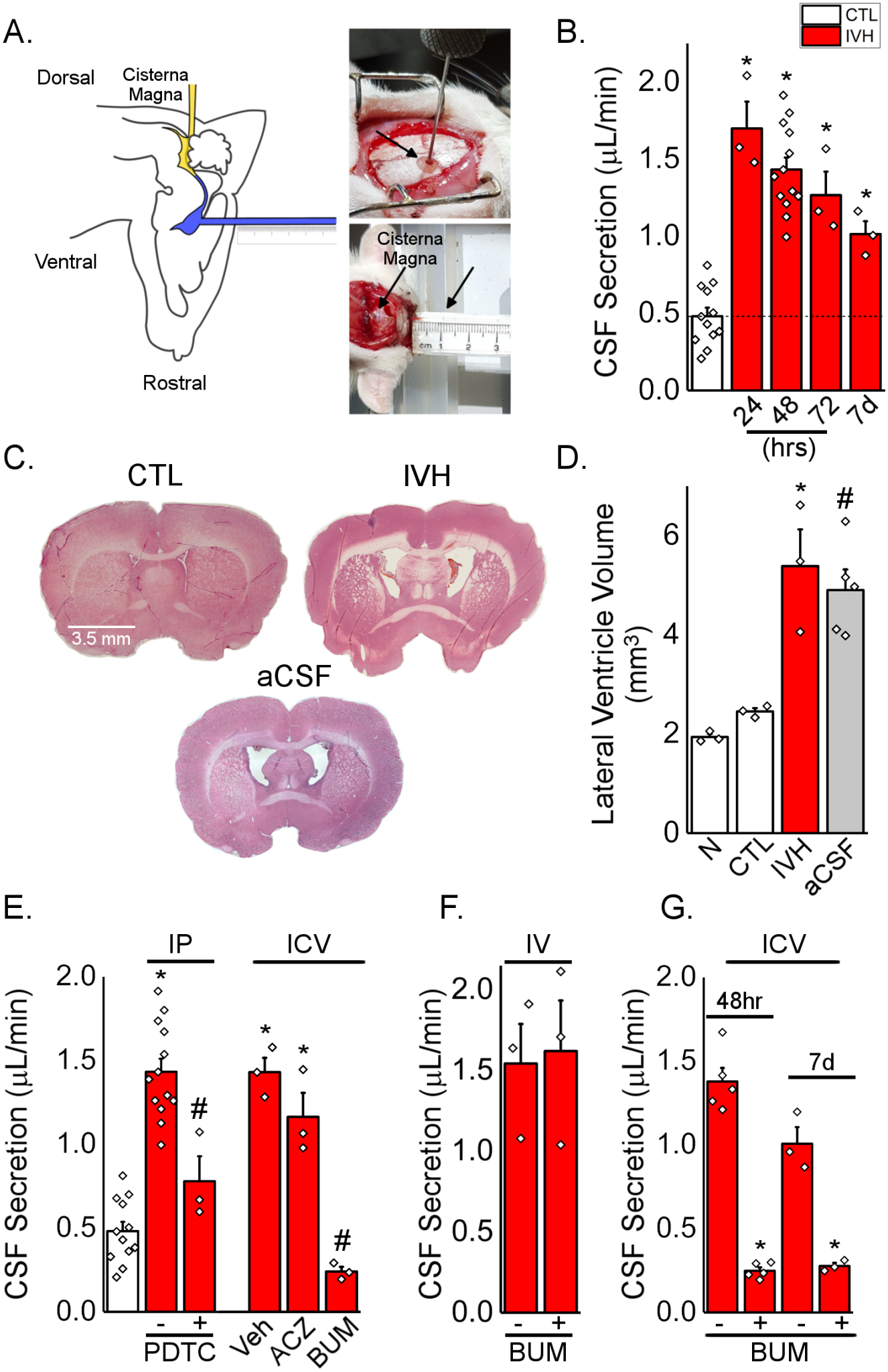
A.
Dorsal
Cisterna Magna
Ventral
Rostral
Cisterna Magna
B.
CTL
IVH
CSF Secretion (µL/min)
2.0
1.5
1.0
0.5
0.0
24
48
72
7d
(hrs)
C.
CTL
IVH
3.5 mm
aCSF
D.
Lateral Ventricle Volume (mm³)
6
4
2
0
N
CTL
IVH
aCSF
E.
IP
ICV
CSF Secretion (µL/min)
2.0
1.5
1.0
0.5
0.0
- +
PDTC
Veh
ACZ
BUM
F.
IV
CSF Secretion (µL/min)
2.0
1.5
1.0
0.5
0.0
- +
BUM
G.
ICV
48hr
7d
CSF Secretion (µL/min)
2.0
1.5
1.0
0.5
0.0
- + - +
BUM

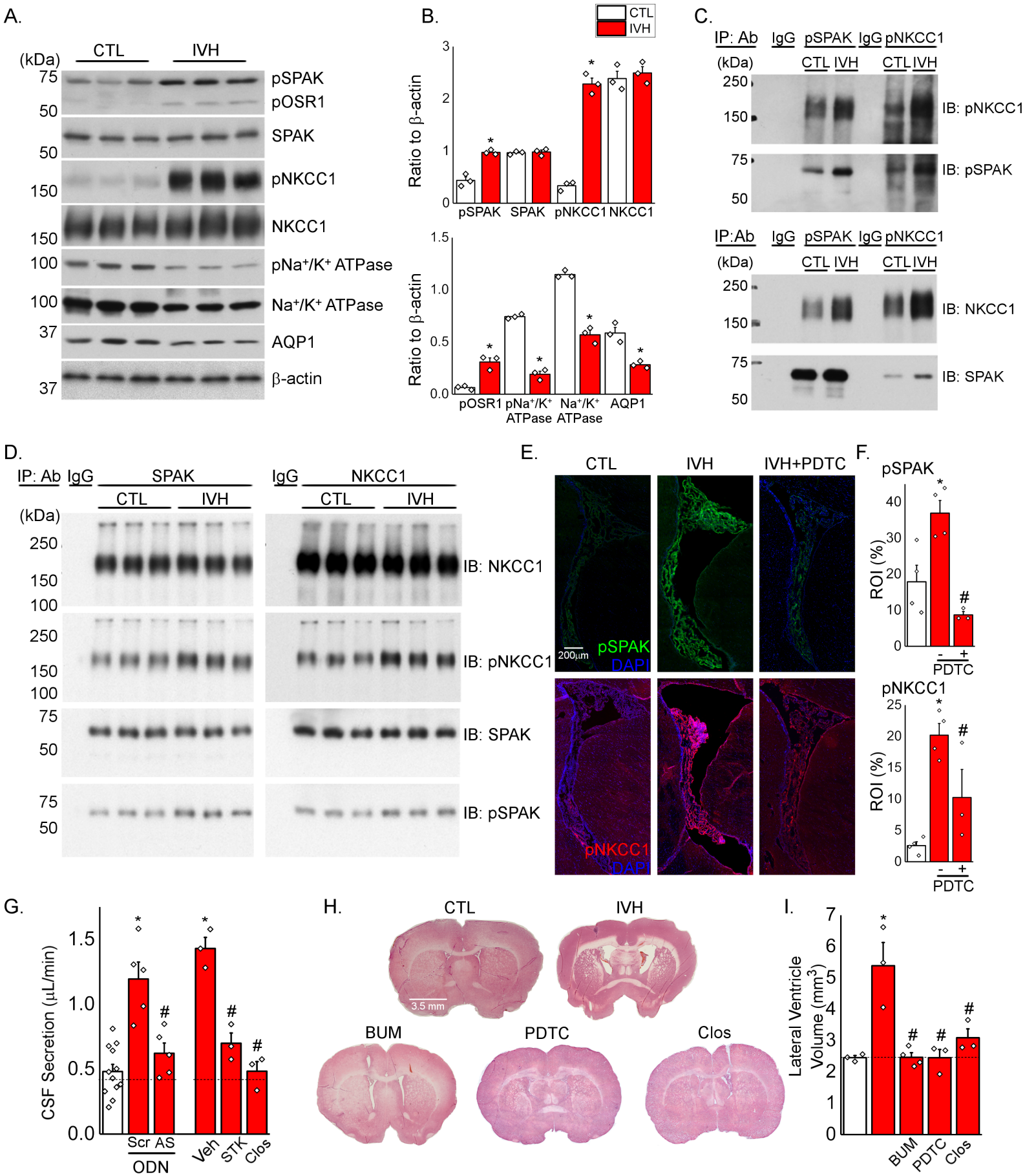
A.
CTL
IVH
(kDa)
75
50
pSPAK
pOSR1
SPAK
150
pNKCC1
NKCC1
100
pNa+/K+ ATPase
Na+/K+ ATPase
37
AQP1
β-actin
B.
CTL
IVH
Ratio to β-actin
pSPAK
SPAK
pNKCC1
NKCC1
pOSR1
pNa+/K+ ATPase
Na+/K+ ATPase
AQP1
C.
IP: Ab
IgG
pSPAK
pNKCC1
IB: pNKCC1
IB: pSPAK
IB: NKCC1
IB: SPAK
D.
SPAK
NKCC1
E.
CTL
IVH
IVH+PDTC
200μm
pSPAK
DAPI
pNKCC1
F.
ROI (%)
PDTC
G.
CSF Secretion (μL/min)
Scr AS ODN
Veh
STK
Clos
H.
3.5 mm
BUM
PDTC
Clos
I.
Lateral Ventricle Volume (mm3)

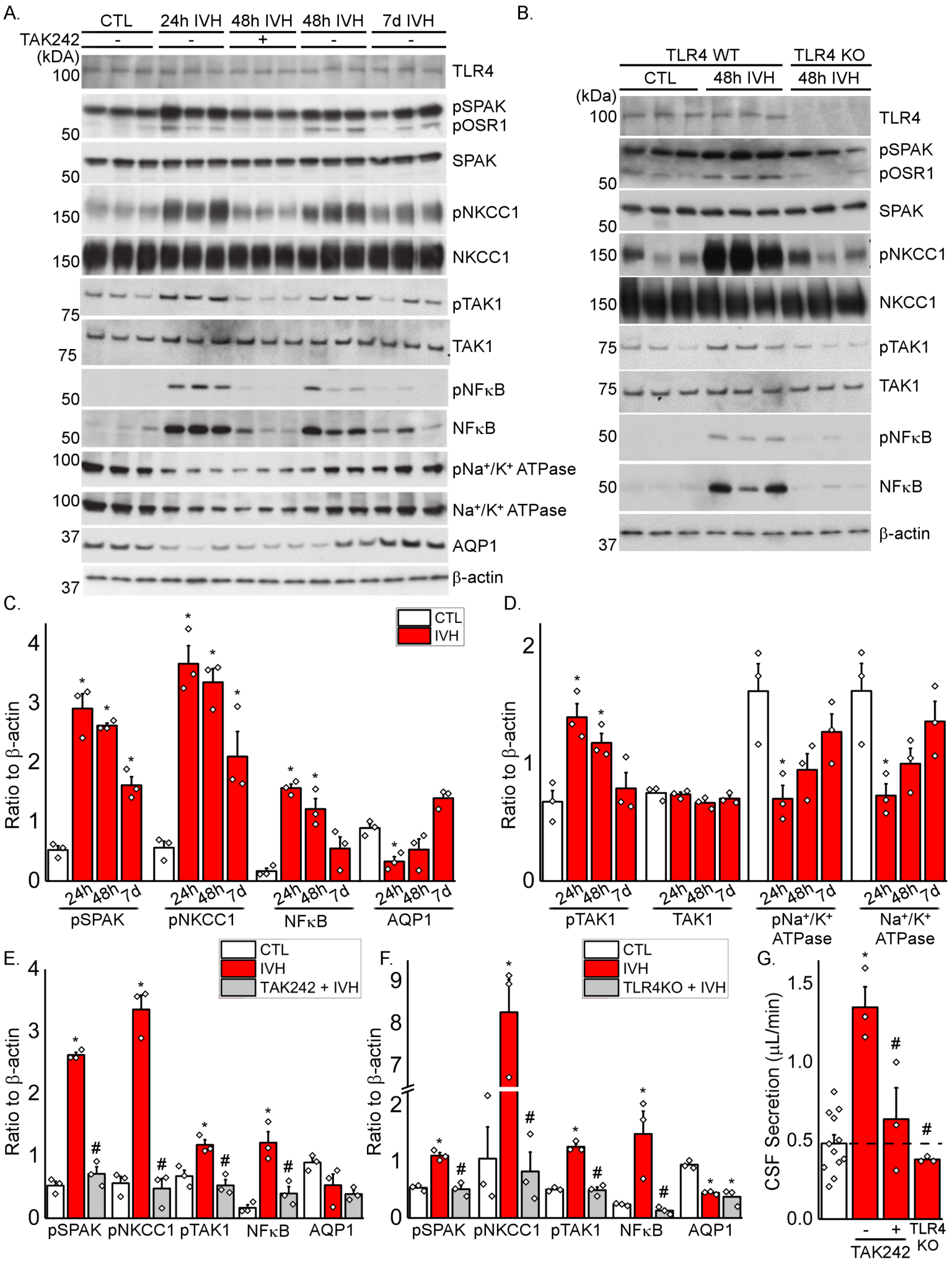
A.
CTL
24h IVH
48h IVH
48h IVH
7d IVH
TAK242
-
-
+
-
-
(kDA)
100
TLR4
pSPAK
pOSR1
50
SPAK
50
150
pNKCC1
150
NKCC1
75
pTAK1
75
TAK1
50
pNFκB
50
NFκB
100
pNa+/K+ ATPase
100
Na+/K+ ATPase
37
AQP1
37
β-actin
B.
TLR4 WT
TLR4 KO
CTL
48h IVH
48h IVH
(kDa)
100
TLR4
pSPAK
pOSR1
50
SPAK
50
150
pNKCC1
150
NKCC1
75
pTAK1
75
TAK1
50
pNFκB
50
NFκB
37
β-actin
C.
CTL
IVH
Ratio to β-actin
0
1
2
3
4
24h 48h 7d
pSPAK
pNKCC1
NFκB
AQP1
D.
Ratio to β-actin
0
1
2
24h 48h 7d
pTAK1
TAK1
pNa+/K+ ATPase
Na+/K+ ATPase
E.
CTL
IVH
TAK242 + IVH
Ratio to β-actin
0
1
2
3
4
pSPAK
pNKCC1
pTAK1
NFκB
AQP1
F.
CTL
IVH
TLR4KO + IVH
Ratio to β-actin
0
1
2
7
8
9
pSPAK
pNKCC1
pTAK1
NFκB
AQP1
G.
CSF Secretion (μL/min)
0.0
0.5
1.0
1.5
-
+
TLR4 KO
TAK242